Time-Varying Climate Sensitivity from Regional Feedbacks

KYLE C. ARMOUR

Department of Earth, Atmospheric, and Planetary Sciences, Massachusetts Institute of Technology, Cambridge, Massachusetts

CECILIA M. BITZ

Department of Atmospheric Sciences, University of Washington, Seattle, Washington

GERARD H. ROE

Department of Earth and Space Sciences, University of Washington, Seattle, Washington

(Manuscript received 31 July 2012, in final form 12 December 2012)

ABSTRACT

The sensitivity of global climate with respect to forcing is generally described in terms of the global climate feedback—the global radiative response per degree of global annual mean surface temperature change. While the global climate feedback is often assumed to be constant, its value—diagnosed from global climate models—shows substantial time variation under transient warming. Here a reformulation of the global climate feedback in terms of its contributions from regional climate feedbacks is proposed, providing a clear physical insight into this behavior. Using (i) a state-of-the-art global climate model and (ii) a low-order energy balance model, it is shown that the global climate feedback is fundamentally linked to the geographic pattern of regional climate feedbacks and the geographic pattern of surface warming at any given time. Time variation of the global climate feedback arises naturally when the pattern of surface warming evolves, actuating feedbacks of different strengths in different regions. This result has substantial implications for the ability to constrain future climate changes from observations of past and present climate states. The regional climate feedbacks formulation also reveals fundamental biases in a widely used method for diagnosing climate sensitivity, feedbacks, and radiative forcing—the regression of the global top-of-atmosphere radiation flux on global surface temperature. Further, it suggests a clear mechanism for the ''efficacies'' of both ocean heat uptake and radiative forcing.

1. Introduction

The response of the earth's climate to changes in forcing is often characterized in terms of the *equilibrium climate sensitivity* ($\equiv\overline{T}_{2\times}$), the global equilibrium surface warming under a doubling of atmospheric CO_2. This definition has facilitated direct comparison of different estimates of climate change, be they instrumental, proxy, or model derived (e.g., Hegerl et al. 2007; Allen et al. 2007; Edwards et al. 2007; Knutti and Hegerl 2008, and references therein). A closely related concept is the *equilibrium global climate feedback* λ_{eq}, defined as the ratio of the global radiative forcing from CO_2 doubling ($\equiv\overline{R}_{2\times}$) to the resulting equilibrium response of global mean surface temperature $\overline{T}_{2\times}$:

$$\lambda_{eq} = -\frac{\overline{R}_{2\times}}{\overline{T}_{2\times}}. \quad (1)$$

Equivalently, λ_{eq} is the global radiative response per degree global mean surface temperature change (units of $W\,m^{-2}\,K^{-1}$) required to reach equilibrium with CO_2 doubling. Thus, λ_{eq} is a measure of the stability of global climate with respect to forcing and a useful diagnostic for long-term climate change (Wigley and Raper 2001; Knutti et al. 2002; Baker and Roe 2009).

On centennial and shorter time scales, the global climate response to forcing is an inherently transient phenomenon that depends on several factors in addition to

Corresponding author address: Kyle Armour, Department of Earth, Atmospheric, and Planetary Sciences, MIT, 54-1526, 77 Massachusetts Ave., Cambridge, MA 02139.
E-mail: karmour@mit.edu

DOI: 10.1175/JCLI-D-12-00544.1

λ_{eq}. The uptake of heat by the deep ocean strongly influences transient warming by acting as a sink of energy at the surface (e.g., Raper et al. 2002). Moreover, the stability of global climate may itself be a variable quantity. We thus define the *effective global climate feedback* λ_{eff} to be the instantaneous global radiative response per degree global mean surface temperature change, where λ_{eff} may be different from λ_{eq} when global climate is out of equilibrium with some forcing.

Climate change on a global scale is widely described through a simple linearization of the global top-of-atmosphere (TOA) energy balance:

$$\overline{H}(t) = \lambda_{eff}(t)\overline{T}(t) + \overline{R}(t), \tag{2}$$

where the global mean energy imbalance $\overline{H}$ is given by the net radiation flux at the TOA, equal to the sum of the radiative forcing $\overline{R}$ (positive downward) and the global radiative response $\lambda_{eff}\overline{T}$ (assumed to be proportional to the global mean surface temperature anomaly $\overline{T}$). Also, $\overline{H}$ may be regarded as the rate of global heat content change, which on decadal and longer time scales is approximately equal to the heat flux into the World Ocean, the primary heat reservoir in the climate system (e.g., Levitus et al. 2001). Each term in Eq. (2) represents a global-mean quantity (denoted by an overbar) and is a function of time t.

Generally λ_{eff} is framed in terms of its corresponding *effective climate sensitivity* (Murphy 1995), defined by

$$\overline{T}_{eff}(t) = -\frac{\overline{R}_{2\times}}{\lambda_{eff}(t)}; \tag{3}$$

$\overline{T}_{eff}$ may be viewed as the climate sensitivity implied by λ_{eff}. Equivalently, $\overline{T}_{eff}$ represents the apparent climate sensitivity as diagnosed by global energy balance [Eq. (2)] at any given time:

$$\overline{T}_{eff}(t) = \frac{\overline{R}_{2\times}}{\overline{R}(t) - \overline{H}(t)}\overline{T}(t). \tag{4}$$

If λ_{eff} is constant, then $\overline{T}_{eff} = -\overline{R}_{2\times}/\lambda_{eq} = \overline{T}_{2\times}$ at all times, and its value can be consistently determined from observations at a variety of time scales. Critically, all observational estimates of $\overline{T}_{2\times}$ rely to some extent on the equivalency of $\overline{T}_{eff}$ and $\overline{T}_{2\times}$.

However, multiple studies have, in fact, shown substantial time variation of λ_{eff} in a wide range of global climate models (GCMs) and forcing scenarios (Murphy 1995; Senior and Mitchell 2000; Watterson 2000; Raper et al. 2002; Boer and Yu 2003a; Gregory et al. 2004; Kiehl et al. 2006; Williams et al. 2008; Winton et al. 2010; Bitz et al. 2012; Li et al. 2013). This implies that $\overline{T}_{eff}$ may be a substantial misdiagnosis of equilibrium climate sensitivity and that observations of climate change from different periods may yield distinct estimates of $\overline{T}_{eff}$, even if a single $\overline{T}_{2\times}$ meaningfully exists in nature. Moreover, knowing how λ_{eff} will evolve presents a major challenge to transient climate prediction.

While the time dependence of λ_{eff} has been widely demonstrated, there is little agreement on the magnitude or mechanism of its variation. Senior and Mitchell (2000) suggest that time-dependent cloud feedbacks arise from interhemispheric warming differences associated with the slow response of the Southern Ocean. Williams et al. (2008) instead argue that the time dependence of $\overline{T}_{eff}$ can be largely accounted for by the use of an ''effective forcing'' in Eq. (4). Recently, Winton et al. (2010) have proposed an alternative interpretation of $\overline{T}_{eff}$ in terms of a time-dependent ''efficacy of ocean heat uptake,'' analogous to the distinct efficacies of different radiative forcing agents wherein each may drive a different global temperature response (per unit global radiative forcing) depending on its geographic forcing structure (e.g., Hansen et al. 1997, 2005; Yoshimori and Broccoli 2008).

Here we propose that λ_{eff} and $\overline{T}_{eff}$ are fundamentally linked to the geographic pattern of regional climate feedbacks and the geographic pattern of surface warming at any given time. Time variation of λ_{eff} emerges naturally as the pattern of warming evolves and regional feedbacks of different strengths are actuated. This principle is demonstrated within (i) a state-of-the-art atmosphere–ocean GCM and (ii) a low-order energy balance climate model. We show that λ_{eff}, usually diagnosed via global energy balance [Eq. (2)], can equivalently be calculated from the instantaneous spatial pattern of surface warming in combination with an estimate of the strength of regional climate feedbacks. The regional feedbacks approach provides a clear, physical interpretation of λ_{eff} and the mechanism of its time variation. These findings are discussed in the context of previous studies, and regional feedbacks are proposed as a mechanism for the efficacy of ocean heat uptake and radiative forcing. Time-varying λ_{eff}, arising from regional climate feedbacks, has important implications for the quantification of radiative forcing, climate feedbacks, and climate sensitivity within both models and observations.

2. Time-varying climate sensitivity from global energy balance

Following previous studies (e.g., Winton et al. 2010) we explore here the time variation of λ_{eff} within an idealized instantaneous CO_2-doubling scenario in which

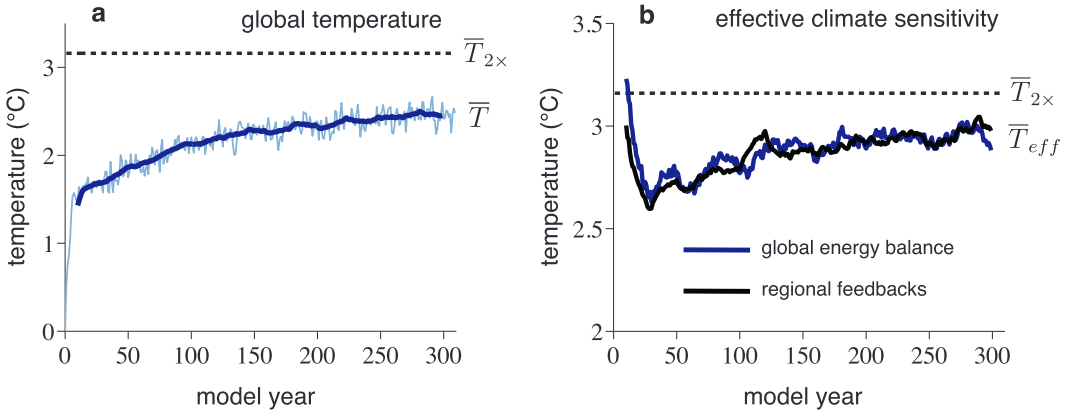

FIG. 1. Evolution of global temperature and effective climate sensitivity within CCSM4: (a) global annual mean surface temperature change $\overline{T}$ and (b) effective climate sensitivity $\overline{T}_{\text{eff}}$ following an abrupt doubling of atmospheric CO_2 in year zero. The $\overline{T}_{\text{eff}}$ diagnosed by global energy balance [Eq. (4)] is shown in blue, and $\overline{T}_{\text{eff}}$ calculated with regional feedbacks [Eq. (8)] is shown in black. Thick lines show 20-yr running means. Equilibrium climate sensitivity $\overline{T}_{2\times}$ is estimated from a slab ocean version of the model.

climate forcing is held constant ($\overline{R} = \overline{R}_{2\times}$) throughout the analysis. We use the fully coupled Community Climate System Model version 4 (CCSM4) (Gent et al. 2011) and measure the perturbed climate state with respect to the long 1850s "control" simulation from which the simulation was branched.

Figure 1a shows the evolution of the global annual-mean surface temperature in CCSM4, along with an estimate of the temperature change $\overline{T}_{2\times}$ that would occur if the model was run to equilibrium; $\overline{T}_{2\times}$ is simulated with a "slab ocean model" (SOM) version of CCSM4 that uses annually repeating ocean heat flux convergence taken from the fully coupled 1850s control simulation (Bitz et al. 2012). The blue line in Fig. 1b shows $\overline{T}_{\text{eff}}$ diagnosed from the global energy balance [Eq. (4)]. Here $\overline{T}_{\text{eff}}$ varies considerably over the simulation, but it is generally less than $\overline{T}_{2\times}$; this behavior is qualitatively similar to that in a wide range of fully-coupled GCMs, though quantitive differences exist across models (Williams et al. 2008; Winton et al. 2010). Because of ocean heat transport changes in the fully coupled integration, it is possible that $\overline{T}$ and $\overline{T}_{\text{eff}}$ may not asymptote to the SOM-estimated value of $\overline{T}_{2\times}$ as equilibrium is approached. Note that the diagnosed $\overline{T}_{\text{eff}}$ is sensitive to the value of CO_2 radiative forcing in Eq. (4). We estimate $\overline{R}_{2\times} = 3.03\ \text{W m}^{-2}$ within CCSM4 based on radiative kernels (see appendix A) and use this value throughout the analysis.

Global energy balance allows a diagnosis of $\overline{T}_{\text{eff}}$ [Eq. (4)] but does not provide insight into why it varies over time. In the following section, we develop a regional feedback framework, from which time dependence of $\overline{T}_{\text{eff}}$ emerges naturally.

3. Time-varying climate sensitivity from regional climate feedbacks

Whereas the global climate feedback is a linearization about the global mean temperature anomaly, feedbacks can be reformulated as a linearization about the local temperature instead (e.g., Boer and Yu 2003a,b; Winton 2006; Bates 2007, 2010; Crook et al. 2011; Boer 2011; Kay et al. 2012). In this formulation, $\lambda(r)$ reflects spatial variations in the relationship between local temperature change $T(r, t)$ and local TOA radiative response, where $r = (\theta, \phi) =$ (latitude, longitude). We make the further assumption that $\lambda(r)$ is time invariant; that is, that the local feedbacks are constant. While we do not expect this assumption to hold in all regions or over a large temperature range, we will show it to be a sufficient description of the global energy budget over the range of climate states considered here.

Climate change at the regional scale is then described in terms of a local energy balance:

$$H(r,t) = \lambda(r)T(r,t) + R(r,t) - \$\,\nabla\mathbf{F}(r,t), \qquad (5)$$

where $H(r, t)$ is the local energy imbalance, equal to the rate of local heat content change; $R(r, t)$ is the local radiative forcing; and $\$\,\nabla\mathbf{F}(r, t)$ represents the change in local horizontal energy divergence because of changes in the combined oceanic and atmospheric heat transport ($\mathbf{F}$).

The global mean of any quantity $Q(r, t)$ is given by

$$\overline{Q}(t) = \frac{1}{4\pi}\int_0^{2\pi}\int_{-\pi/2}^{\pi/2} Q(\theta,\phi,t)\cos\theta\, d\theta\, d\phi, \qquad (6)$$

and we note that $\overline{\$\,\square F} = 0$. Taking the global mean of Eq. (5) must recover the global energy balance described by Eq. (2):

$$\overline{H}(t) = \overline{\lambda(r)T(r,t)} + \overline{R}(t) = \lambda_{\text{eff}}(t)\overline{T}(t) + \overline{R}(t), \quad (7)$$

from which the apparent time dependence of λ_{eff} has been diagnosed in CCSM4 and other models.

From Eq. (7), the identification

$$\lambda_{\text{eff}}(t) = \overline{\lambda(r)\frac{T(r,t)}{\overline{T}(t)}} \quad (8)$$

permits a clean partitioning of λ_{eff} into two physically meaningful factors: the geographic pattern of surface temperature change $T(r,t)/\overline{T}(t)$ and the geographic pattern of regional climate feedbacks $\lambda(r)$. Time-varying climate sensitivity is thus a fundamental consequence of regional climate feedbacks: variations in λ_{eff} occur when the pattern of climate warming evolves and modifies the relative weighting of local feedbacks in Eq. (8) [provided that $\lambda(r)$ varies spatially].

a. Effective climate sensitivity in CCSM4

Can the regional feedbacks framework explain the evolution of $\overline{T}_{\text{eff}}$? If the assumption of constant $\lambda(r)$ is valid, then the full time dependence of $\overline{T}_{\text{eff}}$ is contained in $T(r,t)/\overline{T}(t)$. This factor can be calculated directly from the output of the CCSM4 CO_2-doubling experiment. For $\lambda(r)$ we use the CCSM4 feedbacks calculated using radiative kernels in Bitz et al. (2012) from an equilibrium SOM simulation but normalize the local TOA radiative response by the local temperature change, rather than the global temperature change, to define our local radiative feedbacks.

The effective climate sensitivity $\overline{T}_{\text{eff}}$ calculated from regional feedbacks [Eq. (8)] is in good agreement with that diagnosed from global energy balance (black and blue lines, respectively, in Fig. 1b). This result can equivalently be expressed in terms of λ_{eff} (Fig. 2a). By applying Eq. (8) to the individual climate feedbacks that constitute $\lambda(r)$, λ_{eff} can be partitioned into its various effective feedback components (see Fig. B1 in appendix B). Summing the shortwave (SW) and longwave (LW) effective feedbacks separately shows that both contribute to the overall time variation of λ_{eff} (Fig. 2a). Moreover, each is in good agreement with its corresponding effective feedback as diagnosed from global energy balance, although it appears that a portion of the SW feedback time variation is not captured over the first few decades of the integration. Correspondingly, the calculated effective feedbacks are largely able to represent the nonlinear evolution of SW, LW, and net global TOA radiation fluxes with global annual mean surface temperature (Fig. 2b).

The above results are a measure of the success of the fundamental assumptions and approximations that we have made regarding local feedbacks. Since $\lambda(r)$ was defined in terms of local surface temperature change only, we have neglected (i) nonlocal contributions to climate feedbacks (e.g., nonlocal influences on cloud or lapse rate changes under transient warming) and (ii) nonlinear contributions to local feedbacks that may arise due to higher-order temperature dependencies.

We have made the further approximation that feedbacks calculated from the slab ocean model using linear radiative kernel feedback decomposition may be employed for the estimation of local feedbacks within CCSM4 under transient warming. As is usual for linear feedback analysis, we have neglected correlations between feedbacks (e.g., due to the relationship between sea ice and the overlying lapse rate or cloud cover) and other radiative elements not included in the feedback decomposition. Moreover, while the local feedbacks have been calculated using radiative kernels constructed at each vertical atmospheric level and for each month (e.g., Soden and Held 2006; Shell et al. 2008), Eq. (8) approximates local feedbacks as functions of local annual mean surface temperature change, and thus it neglects a potential source of time dependence arising from any variations in the vertical structure of warming or seasonality that do not scale linearly with annual mean surface temperature over the integration. Finally, cloud feedbacks have been estimated using the "adjusted cloud radiative forcing" method (Soden et al. 2008; Shell et al. 2008), which does not distinguish the mechanisms of cloud changes, and thus may be biased by forcing-induced cloud changes that occur prior to the surface temperature response (appendix A).[1]

Further work is necessary to quantify the full consequences of the above approximations and assess the range of climate states over which they hold. However, the results of Figs. 1b and 2 suggest that $\overline{T}_{\text{eff}}$ (and the corresponding λ_{eff}) may be largely explained in terms of the geographic pattern of surface temperature at any given time through the "actuation" of local, time-invariant climate feedbacks: although local feedbacks are continuously operating, the contribution of any region to the global effective feedback depends directly on the magnitude of regional temperature change [Eq. (8)].

[1] "Adjusted" here refers to accounting for the effects of cloud masking on noncloud feedbacks and should not be confused with allowing for fast tropospheric adjustment in estimates of forcing.

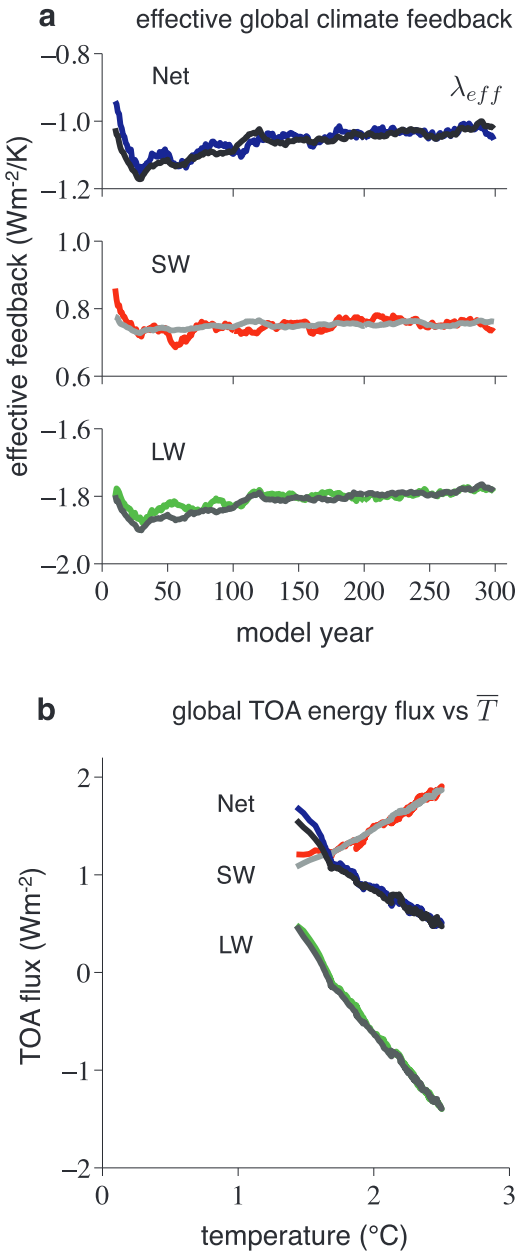

FIG. 2. Evolution of global effective climate feedbacks and global TOA energy fluxes within CCSM4: (a) net, SW, and LW effective climate feedbacks diagnosed from global energy balance [Eq. (2); blue, red, and green, respectively] and calculated with regional feedbacks [Eq. (8); black, light gray, and dark gray, respectively] and (b) global net, SW, and LW TOA radiation flux as a function of global annual mean surface temperature change from the simulation (blue, red, and green respectively) and as predicted from Eq. (2) using the calculated effective feedbacks (black, light gray, and dark gray, respectively). See appendix A for the CO_2 radiative forcing employed here. All lines show 20-yr running means.

Thus, the link between global warming and radiative response (the fundamental control on the stability of global climate) inherently depends on the geographic structure of warming. When regional feedbacks are defined in the conventional way (i.e., normalized with respect to $\overline{T}$), they will inevitably vary in magnitude as the geographic pattern of surface warming evolves, even without any change in the local physics linking the TOA radiation and surface temperature. Imposing a global view of climate sensitivity and feedbacks makes the climate response to forcing appear more complicated than it truly is. In many respects then, the local feedbacks formulation is to be preferred.

GEOGRAPHIC PATTERNS OF WARMING AND FEEDBACKS

So far, we have found that $\overline{T}_{\text{eff}}$ depends on (i) the spatial pattern of warming and (ii) the spatial pattern of local feedbacks, and verified that Eq. (8) largely accounts for the evolution of $\overline{T}_{\text{eff}}$. We next analyze the two factors in Eq. (8) and focus on several distinctive time intervals that can be identified from Fig. 1b. The evolution of the pattern of global warming, $T(r,t)/\overline{T}(t)$, during these intervals is shown in Fig. 3. Following CO_2 doubling,

(i) within several years (years 1–10; Fig. 3a) temperatures adjust over land and sea ice, consistent with the relatively small heat capacities of these climate components.

(ii) Over the following decades (years 1–10 to years 20–60; Fig. 3b) warming is characterized by a more globally uniform pattern, with substantial warming of the tropical oceans and a reduced land–ocean warming contrast. On these decadal time scales, the ocean plays a primary role in setting regional temperature trends. Reduced northward ocean heat transport in the North Atlantic Ocean may contribute to local cooling, while increased ocean heat transport into the Arctic Ocean may enhance sea ice loss (Bitz et al. 2006; Holland et al. 2006). Delayed surface warming in the Southern Ocean may be driven by a combination of factors, including upwelling of unmodified water from depth, decreased southward ocean heat transport (Bitz et al. 2006), and reduced upward isopycnal mixing of heat into the mixed layer due to weakened convection (Gregory 2000; Bitz et al. 2006; Kirkman and Bitz 2011).

(iii) Over the following centuries (years 20–60 to years 200–300; Fig. 3c), a pattern of polar-amplified warming emerges in both hemispheres as global climate slowly attains equilibrium with the imposed forcing (Manabe et al. 1991; Holland and Bitz 2003; Stouffer 2004).

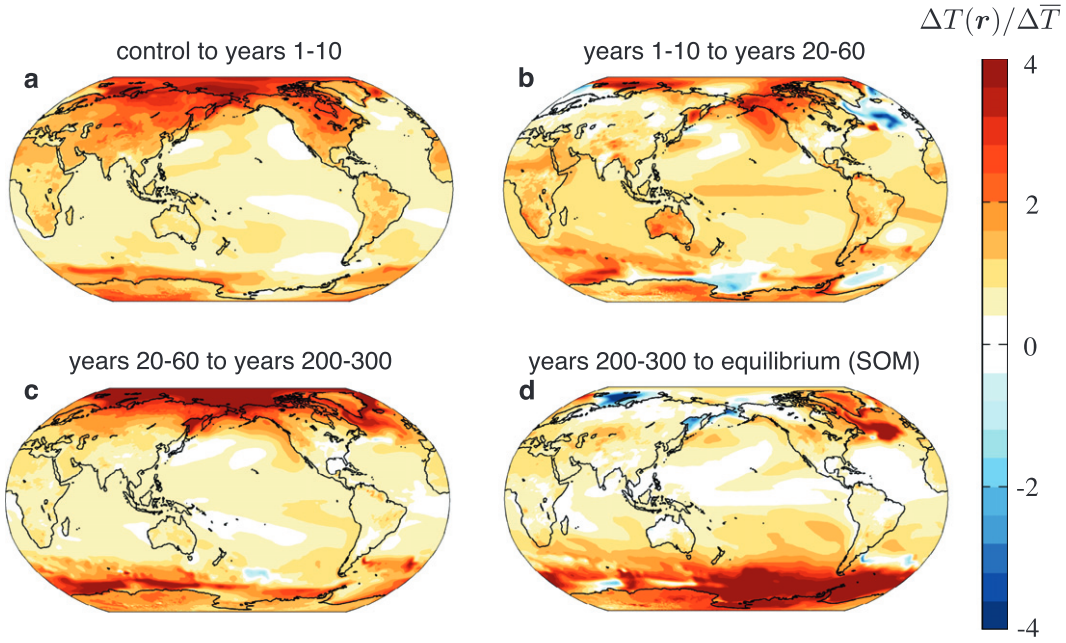

FIG. 3. Spatial patterns of warming within CCSM4: regional surface temperature change normalized by global-mean surface temperature change between the periods (a) "control" to years 1–10, (b) years 1–10 to 20–60, (c) years 20–60 to 200–300, and (d) years 200–300 to equilibrium (as estimated by the SOM).

(iv) For completeness, we also show the temperature change from years 200–300 to the equilibrium defined by the SOM (Fig. 3d). The differences are characterized by further high-latitude warming, notably in the Southern Ocean and in the North Atlantic Ocean, both regions that had shown little warming to that point.

These basic patterns can also be seen in the zonal means (Fig. 4a) and are broadly consistent with those found within other GCM simulations of transient climate warming (e.g., Manabe et al. 1991; Stouffer 2004; Held et al. 2010).

Next we present the spatial pattern of the net regional feedback $\lambda(r)$ together with its partitioning into individual feedbacks in Fig. 5. Many of the important features can also be seen in the zonal means of the feedbacks, which are given in Fig. 4b. The net feedback is generally strongly negative (stabilizing) in the low to midlatitudes (particularly over the oceans), owing to locally large and negative Planck and lapse rate feedbacks (Figs. 5b,e). The net feedback becomes less negative (less stabilizing) toward high latitudes, due mainly to less-negative Planck and lapse rate feedbacks, though this is partially offset by a less-positive water vapor feedback at high latitudes (Fig. 5c). In the Arctic and Southern Oceans, $\lambda(r)$ becomes locally positive owing to local maxima in surface albedo and lapse rate feedbacks (Figs. 5e,f). The net feedback is generally less negative over land, compared to the oceans, because of (i) reduced Planck and lapse rate feedbacks over land at any given latitude and (ii) positive snow albedo feedbacks, particularly in the Northern Hemisphere (Figs. 5b,e,f). Finally, cloud feedbacks are characterized by substantial spatial variability (Figs. 5g,h) but contribute relatively little to the equator-to-pole net feedback structure (Fig. 4b).

The temporal and spatial patterns presented in Figs. 3–5 can be combined via Eq. (8) to yield a clear understanding of the time variation of $\overline{T}_{\text{eff}}$.

(i) Immediately following CO_2 doubling, warming over land and sea ice, in the presence of more-positive-than-average regional climate feedbacks, drives an initially high value of $\overline{T}_{\text{eff}}$.
(ii) Over the following decades the tropical oceans warm, actuating large and negative (stabilizing) tropical feedbacks and reducing $\overline{T}_{\text{eff}}$.
(iii) Over succeeding centuries the slow emergence of polar-amplified warming, in the presence of less-negative (or even locally positive) high-latitude feedbacks, increases $\overline{T}_{\text{eff}}$ toward $\overline{T}_{2\times}$.
(iv) Eventually $\overline{T}_{\text{eff}}$ would asymptote to a value that depends on the geographic pattern of surface warming at equilibrium. Ocean heat transport changes in the coupled model that influence the equilibrium warming pattern may thus drive a value of $\overline{T}_{2\times}$ that is distinct from that estimated by the SOM.

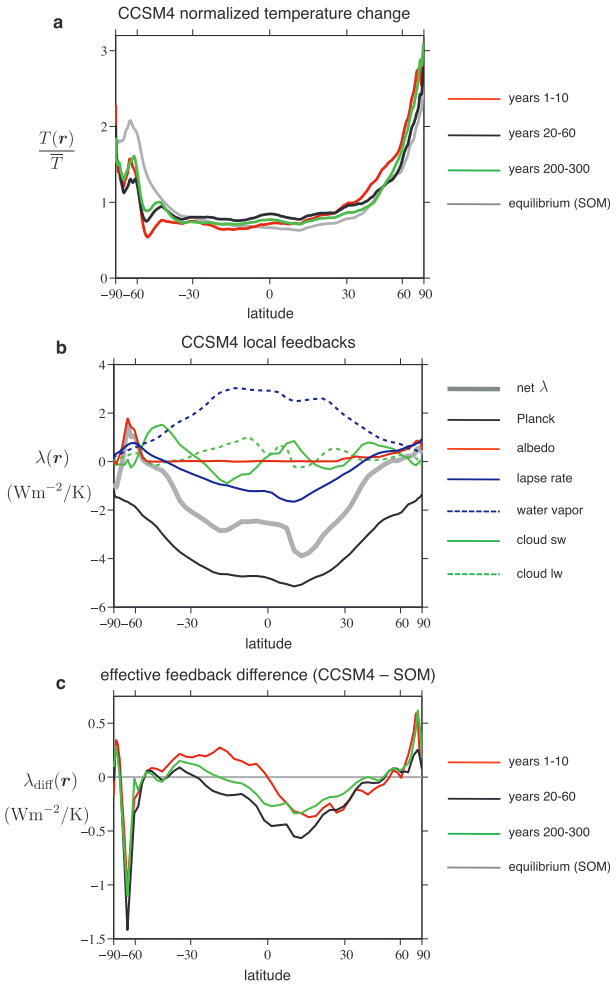

FIG. 4. Zonal-mean warming and local feedbacks within CCSM4: (a) regional surface temperature change normalized by global mean surface temperature change; (b) local net feedback (gray) and individual feedbacks, as in Fig. 5—the individual feedbacks everywhere sum to the net feedback $\lambda(r)$; and (c) effective feedback from CCSM4 minus effective feedback from the SOM—the area-weighted global mean of each curve is equal to $\lambda_{\text{eff}} - \lambda_{\text{eq}}$.

Many of the important features in the foregoing arguments can be seen in the zonal means of $T(r,t)/\overline{T}(t)$ and $\lambda(r)$ (Figs. 4a,b). A quantity of interest is the difference between the effective local feedbacks [which vary with patterns of transient warming, $T(r,t)$] and the equilibrium local feedbacks [which are determined by the pattern of equilibrium warming ($\equiv T(r)_{2\times}$)]:

$$\lambda_{\text{diff}}(r,t) = \lambda(r)T(r,t)/\overline{T}(t) - \lambda(r)T(r)_{2\times}/\overline{T}_{2\times}. \quad (9)$$

From Eq. (8) the global mean of $\lambda_{\text{diff}}(r, t)$ at any given time is equal to $\lambda_{\text{eff}}(t) - \lambda_{\text{eq}}$. The zonal mean of $\lambda_{\text{diff}}(r, t)$ for the distinct time periods considered here is shown in Fig. 4c. Delayed surface warming within the Southern Ocean results in substantially less positive effective local feedbacks compared to equilibrium. Similarly, rapid surface warming in the tropics combined with strongly negative local feedbacks results in more negative tropical effective feedbacks. Finally, enhanced warming in the Arctic (due to changes in ocean circulation not accounted for in the SOM, which are strongly amplified by sea ice changes; see Fig. 3d) leads to more positive Arctic effective feedbacks under transient warming.

In summary, $\overline{T}_{\text{eff}}$ is less than $\overline{T}_{2\times}$ under transient warming due to relatively rapid warming toward equilibrium in low-latitude regions, in the presence of large negative local feedbacks, and to relatively slow warming in mid-to-high latitude regions (particularly in the Southern Hemisphere), in the presence of less-negative local feedbacks. The results thus suggest that to understand $\overline{T}_{\text{eff}}$ one needs only to understand the time scales of regional temperature change and the local feedbacks. This highlights the importance of efforts to identify the underlying principles of regional feedbacks and temperature response in models and nature. In the next section we explore a minimalist model representing distinct climatic regions, which provides insight into the behavior of a commonly used metric for estimating global climate sensitivity, feedbacks, and forcing.

b. *Effective climate sensitivity in a low-order energy balance climate model*

As a parsimonious demonstration of time-varying $\overline{T}_{\text{eff}}$ from regional climate feedbacks, consider a simple model wherein the earth is represented by three regions of equal area, each described by a local energy balance [Eq. (5)]. We associate these regions with land, low-latitude oceans (low), and high-latitude oceans (high), and choose properties of each to broadly mimic the distinct geographic patterns of surface warming and feedbacks identified previously. That is, we set $-\lambda_{\text{high}} < -\lambda_{\text{land}} < -\lambda_{\text{low}}$ as in Fig. 5a. For simplicity, we assume a constant heat capacity for each region, with values c_{land} □ $c_{\text{low}} < c_{\text{high}}$ chosen to simulate the fast response of land and slow response of the high latitudes as in Fig. 3. These basic ingredients are sufficient to qualitatively reproduce the time dependence of $\overline{T}_{\text{eff}}$ within GCMs.

Table 1 summarizes the model parameters and their numerical values, though these exact values are less important than the principle of their interaction. We additionally prescribe the same value of radiative forcing in each region and neglect changes in heat transport between regions. The three-region model, similar in form to those used previously (e.g., Bates 2007, 2010), is then described simply by

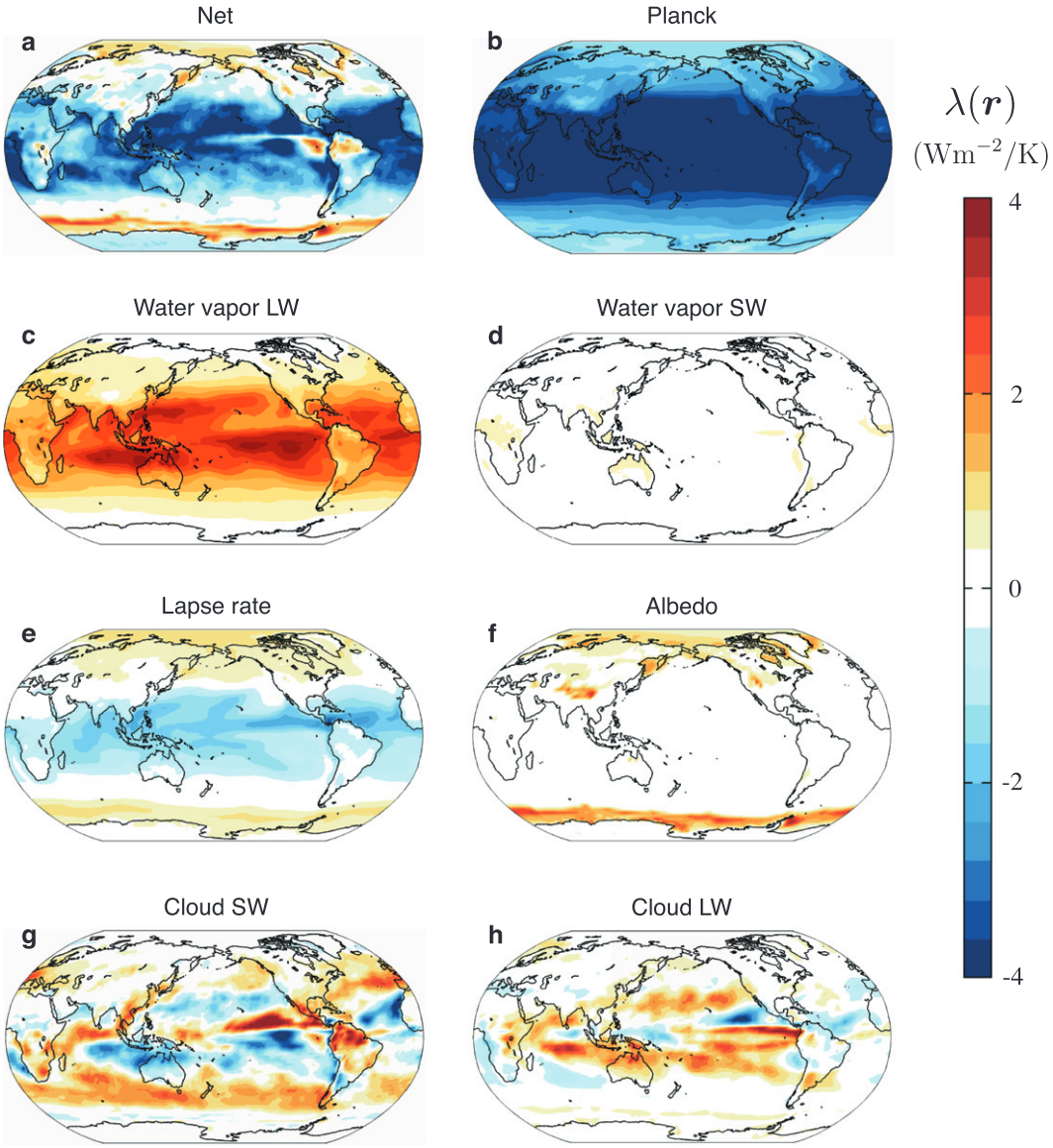

FIG. 5. Spatial patterns of net and individual local feedbacks within CCSM4: local feedbacks (local TOA response per degree local surface temperature change) separated into (a) net (sum of all individual feedbacks), (b) Planck, (c) LW water vapor, (d) SW water vapor, (e) lapse rate, (f) surface albedo, (g) cloud SW, and (h) cloud LW feedbacks.

$$c_{\text{land}}\frac{dT_{\text{land}}}{dt} = H_{\text{land}} = \lambda_{\text{land}}T_{\text{land}} + R,$$
$$c_{\text{low}}\frac{dT_{\text{low}}}{dt} = H_{\text{low}} = \lambda_{\text{low}}T_{\text{low}} + R,$$
$$c_{\text{high}}\frac{dT_{\text{high}}}{dt} = H_{\text{high}} = \lambda_{\text{high}}T_{\text{high}} + R. \qquad (10)$$

The response to an instantaneous CO_2 doubling is characterized by fast warming over land, slow warming over low-latitude oceans, and very slow warming over high-latitude oceans (Fig. 6a). The resulting λ_{eff}, calculated by either the global energy balance [Eq. (2)] or, equivalently, by regional feedbacks [Eq. (8)]

$$\lambda_{\text{eff}}(t) = 1/3\ \left[\lambda_{\text{land}}\frac{T_{\text{land}}(t)}{\overline{T}(t)} + \lambda_{\text{low}}\frac{T_{\text{low}}(t)}{\overline{T}(t)} + \lambda_{\text{high}}\frac{T_{\text{high}}(t)}{\overline{T}(t)}\right], \qquad (11)$$

corresponds to an evolution of $\overline{T}_{\text{eff}}$ (Fig. 6b) that is qualitatively similar to that in CCSM4 (Fig. 1b). This

TABLE 1. Three-region energy balance climate model parameters and regional equilibrium temperature response. We characterize each region by an ocean layer of effective depth h, density ρ, and specific heat C_p, and thus set $c = \rho C_p h$ in Eq. (10). We assume the same radiative forcing: $R = 3\,\mathrm{W\,m^{-2}}$ in each region.

		Region		
Model parameter	Symbol	Land	Low	High
Effective ocean depth (m)	h	5	150	1500
Local feedback ($\mathrm{W\,m^{-2}\,K^{-1}}$)	λ	−0.86	−2.00	−0.67
Equilibrium warming (°C)	$-R/\lambda$	3.5	1.5	4.5

behavior can be understood simply in terms of the weighting of each of the regional feedbacks in Eq. (11) by the evolving pattern of surface warming shown in Fig. 6c.

The details of $\overline{T}_{\mathrm{eff}}$ are sensitive to the model and parameter choices we that have made. However, time variation of $\overline{T}_{\mathrm{eff}}$ is an inevitable result, given an evolving geographic pattern of warming in conjunction with a spatial pattern of regional feedbacks [i.e., Eq. (8)]. By resolving three distinct regions and their associated time scales of response, the simple model is able to capture the main features of the $\overline{T}_{\mathrm{eff}}$ evolution as simulated by GCMs. A minimum of three regions is necessary for characterizing the behavior in Fig. 1b; a model with only one region would simulate constant $\overline{T}_{\mathrm{eff}} = \overline{T}_{2\times}$, while a model with two distinct regions would only be able to simulate a monotonically increasing or decreasing $\overline{T}_{\mathrm{eff}}$. A model with a larger number of regions, or greater complexity (e.g., a representation of time-dependent heat capacities or changes in heat transport between regions), could capture the finer details of $\overline{T}_{\mathrm{eff}}$ variation.

Finally, since it is typically too expensive to run fully coupled models to equilibrium, a commonly used diagnostic for climate sensitivity, feedbacks, and forcing is a scatterplot of the global TOA flux $\overline{H}$ versus the global surface temperature $\overline{T}$, as it evolves during the model integration (e.g., Gregory et al. 2004). Figure 6d shows this scatterplot for the minimalist model. If λ_{eff} was constant, then the relationship between $\overline{H}$ and $\overline{T}$ (under constant $\overline{R} = \overline{R}_{2\times}$) would be linear [Eq. (2)], and the trajectory of points would follow the thick dashed line, with slope $\lambda_{\mathrm{eq}} = -\overline{R}_{2\times}/\overline{T}_{2\times}$. However, since λ_{eff} is not constant [Eq. (11)], we expect this assumption not to hold, and indeed Fig. 6d shows substantial departure from linear behavior. The intersection of the thin dashed line, through the points $[0, \overline{R}_{2\times}]$ and $[\overline{T}(t), \overline{H}(t)]$, with the $\overline{T}$-axis maps out $\overline{T}_{\mathrm{eff}}$ as it evolves over the simulation (Fig. 6b). The slope of this line is thus $\lambda_{\mathrm{eff}} = -\overline{R}_{2\times}/\overline{T}_{\mathrm{eff}}$.

How, then, should the slope of the $\overline{H}$–$\overline{T}$ regression be interpreted, and why does it evolve over the course of the integration? From Eq. (7) the instantaneous slope is given by

$$\frac{d\overline{H}}{d\overline{T}} = \frac{d}{d\overline{T}}\overline{\lambda(r)T(r,t)} = \overline{\lambda(r)\frac{dT(r,t)}{d\overline{T}(t)}} \tag{12}$$

and is thus a measure of the strength of regional feedbacks weighted by the rate of local temperature change with global temperature change. For the three-region model, the slope

$$\frac{d\overline{H}}{d\overline{T}} = 1/3\ \left[\lambda_{\mathrm{land}}\frac{dT_{\mathrm{land}}}{d\overline{T}} + \lambda_{\mathrm{low}}\frac{dT_{\mathrm{low}}}{d\overline{T}} + \lambda_{\mathrm{high}}\frac{dT_{\mathrm{high}}}{d\overline{T}}\right] \tag{13}$$

is weighted toward the land feedback in the initial years, toward the low-latitude ocean feedback in subsequent decades, and finally toward the high-latitude ocean feedback in subsequent centuries (Fig. 6a). Beyond a few centuries, only the high-latitude ocean region is still warming substantially, giving $d\overline{H}/d\overline{T} \approx \lambda_{\mathrm{high}}$. In this regime, the $\overline{H}$–$\overline{T}$ regression line (solid line in Fig. 6d) may be extrapolated (with slope λ_{high}) to the point $[\overline{T}_{2\times}, 0]$ to estimate $\overline{T}_{2\times}$ even before the global equilibrium has been reached.

The blue line in Fig. 2b shows the equivalent scatterplot results from the CCSM4 integration. Reproduced in greater detail in Fig. 7, the scatterplot shows similar behavior to the minimalist model. Late in the simulation, the points appear to evolve along a linear trajectory (solid black regression line), suggesting a regime in which the surface temperature evolves with a fixed spatial pattern [i.e., $dT(r,t)/d\overline{T}(t)$, and thus $d\overline{H}/d\overline{T}$, is constant]. Under the assumption that this linear trajectory continues to equilibrium, the regression line may be extrapolated to the $\overline{T}$ axis to give an estimate of the fully coupled model climate sensitivity that is similar to the SOM-estimated value $\overline{T}_{2\times}$, consistent with Danabasoglu and Gent (2008). While this method is commonly used to estimate $\overline{T}_{2\times}$ within fully coupled GCMs, it is important to emphasize that the slope of the regression is not a measure of λ_{eq} or λ_{eff}. Moreover, the intercept of the regression line with the $\overline{H}$ axis is not a measure of $\overline{R}_{2\times}$. In the following section we discuss the implications of this result for the calculation of climate sensitivity, feedbacks, and forcing from regression methods.

4. Connection to previous studies

As reviewed in the introduction, the time dependence of $\overline{T}_{\mathrm{eff}}$ has been noted previously, and various different mechanisms for its behavior have been proposed. Our physical interpretation via Eq. (8) can be compared to these previous studies.

Senior and Mitchell (2000) highlight time-dependent cloud feedbacks, arising from interhemispheric warming

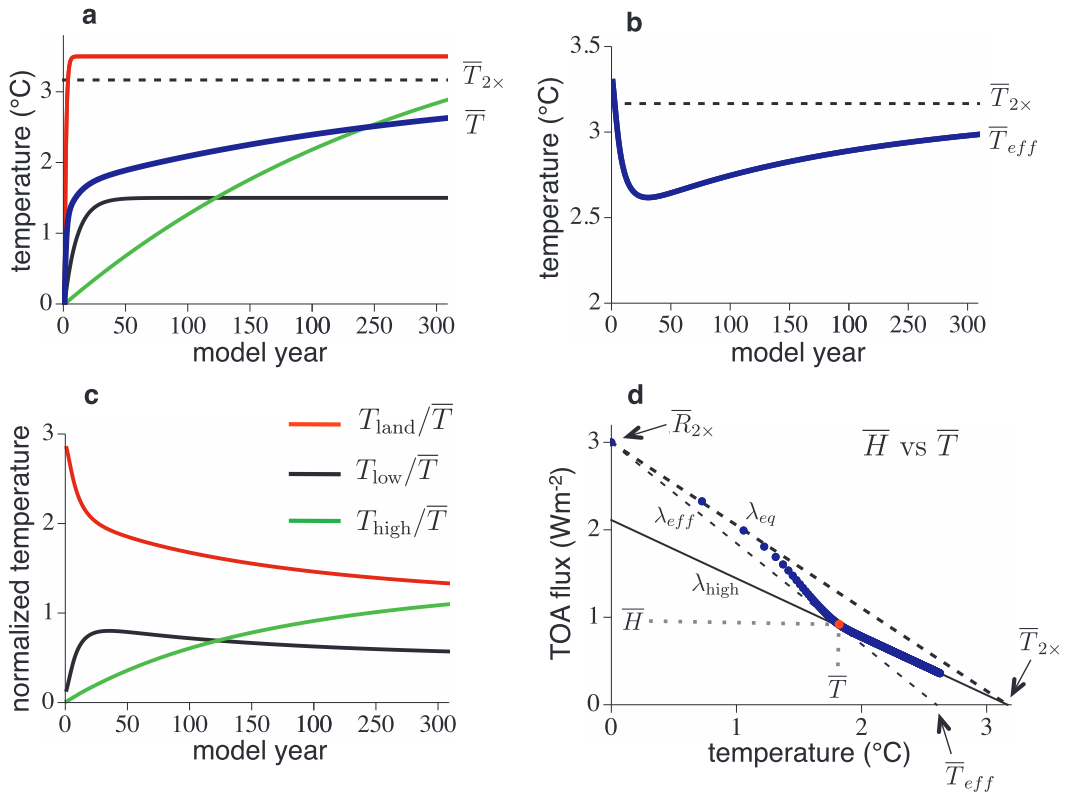

FIG. 6. Temperature and effective climate sensitivity in a three-region energy balance climate model: (a) global mean (blue), land (red), low-latitude ocean (black), and high-latitude ocean (green) surface temperature change following an abrupt doubling of CO_2 in year zero; (b) effective climate sensitivity; (c) regional temperature change normalized by global mean temperature change; and (d) global TOA energy flux plotted against global mean temperature change. The red dot indicates a particular year with global energy flux equal to $\overline{H}$ and global-mean temperature equal to $\overline{T}$. The $\overline{T}_{\rm eff}$ at this time can be schematically represented as the extrapolation of the thin dashed line (with slope $\lambda_{\rm eff}$) from point $(0, \overline{R}_{2\times})$ through this dot to the $\overline{T}$ axis. Late in the simulation, $\overline{T}_{2\times}$ can be estimated by extrapolating a regression line (solid line with slope $\lambda_{\rm high}$) to the $\overline{T}$ axis. The thick-dashed line (with slope $\lambda_{\rm eq}$) connecting points $(0, \overline{R}_{2\times})$ and $(\overline{T}_{2\times}, 0)$ is the expected trajectory of points under the assumption that $\overline{T}_{\rm eff}$ is constant.

differences associated with the slow response of the Southern Ocean, as a chief cause of time dependence in $\lambda_{\rm eff}$. The slow emergence of high-latitude warming (Fig. 3), particularly in the Southern Hemisphere, certainly plays a central role in the delayed actuation of high-latitude feedbacks within CCSM4. However, each individual feedback contributes to $\lambda_{\rm eff}$ through $\lambda(r)$ in Eq. (8), and it is those feedbacks with the greatest meridional structure that contribute most to the time variation of $\lambda_{\rm eff}$ as the polar-amplified warming pattern emerges. Less negative Planck and lapse rate feedbacks in high latitudes, compared to low-latitude regions, are the chief contributors to the meridional structure in $\lambda(r)$, while the surface albedo feedback contributes locally in the Arctic and Southern Ocean, and the water vapor feedback opposes the net feedback meridional structure (Fig. 4b). As a result, each of these effective feedbacks varies substantially over the integration while, in contrast, cloud feedbacks appear to play a smaller role in the time-variation of $\lambda_{\rm eff}$ (Fig. B1) owing to their relatively weak meridional structure (Fig. 4b).

The above finding is at odds with those of Senior and Mitchell (2000) and with others (e.g., Andrews et al. 2012b) who find a nonlinear relationship between global cloud radiative forcing (CRF) and global surface temperature in a range of GCMs. As noted previously, while Eq. (8) accounts for much of the time variation of $\lambda_{\rm eff}$ as diagnosed via global energy balance, there is a portion of the variation, particularly in the SW over the first few decades, that is not captured (Fig. 2a). It is thus plausible that we have neglected a source of time variation in the effective SW cloud feedback that has been identified in these previous studies, possibly due to nonlinear or nonlocal feedback dependencies, or owing to biases in our estimated pattern of local SW cloud feedbacks. Future efforts to reconcile these results should also

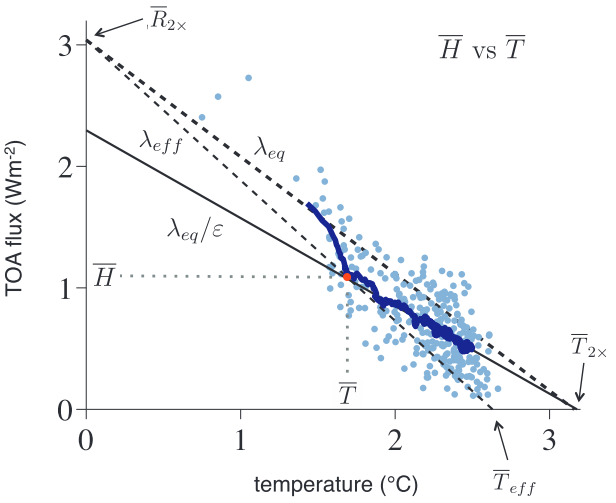

FIG. 7. CCSM4 TOA energy flux plotted against global annual mean temperature change. Light blue dots show individual years, and the dark blue line shows the 20-yr running mean. The red dot indicates a particular decade with global energy flux equal to $\overline{H}$ and global-mean temperature equal to $\overline{T}$. The $\overline{T}_{\text{eff}}$ at this time can be schematically represented as the extrapolation of the thin dashed line (with slope λ_{eff}) from point (0, $\overline{R}_{2\times}$) through this dot to the $\overline{T}$ axis. Late in the simulation, $\overline{T}_{2\times}$ can be estimated by extrapolating a regression line (solid line with slope $\lambda_{\text{eq}}/\varepsilon$) to the $\overline{T}$ axis. The regression is performed over the final two centuries of the simulation.

consider that different methods of estimating cloud feedbacks may also play a role (e.g., accounting for cloud masking effects here as opposed to using an unmodified CRF as in Andrews et al. 2012b).

Williams et al. (2008) argue that the time dependence of $\overline{T}_{\text{eff}}$ can be accounted for by an "effective forcing" that includes those climate responses that are fast compared to the period of slow climate equilibration; these include stratospheric and tropospheric adjustments, as well as warming over land, sea ice, and regions of the ocean. The basic reasoning is that a misdiagnosis of $\overline{R}$ can lead to an apparent time dependence in λ_{eff} in Eq. (2) whereas none would otherwise exist. Performing $\overline{H}$–$\overline{T}$ regression in a range of GCMs, Williams et al. (2008) note a generally strong linearity as equilibrium is approached (as seen for CCSM4 in Fig. 7) and propose that the slope of this regression gives an estimate of λ_{eq}, provided that we interpret the intercept of this line with the $\overline{H}$ axis as the effective forcing and the intercept with the $\overline{T}$ axis as $\overline{T}_{2\times}$ (solid line in Fig. 7). In this interpretation, then, the time-dependence of λ_{eff} appears to be largely eliminated over the stabilization period (Williams et al. 2008). This method has been widely applied to estimate feedbacks and forcing within both models and observations (Forster and Taylor 2006; Forster and Gregory 2006; Gregory and Webb 2008; Andrews and Forster 2008; Williams et al. 2008; Murphy et al. 2009; Boer 2011; Crook et al. 2011; Andrews et al. 2012a; Andrews et al. 2012b; Webb et al. 2013).

Here, we employ an interpretation of "forcing" as those TOA flux changes that occur independent of and prior to any surface temperature response to CO_2, and of "feedbacks" as those TOA flux changes that scale with surface temperature. The relevant forcing then includes stratospheric adjustments as well as any semidirect, tropospheric adjustments occurring on time scales of days to weeks (Gregory and Webb 2008; Andrews and Forster 2008; Williams et al. 2008; Colman and McAvaney 2008; Andrews et al. 2012a; Webb et al. 2013); importantly, the forcing excludes surface temperature changes. In this view, it is generally not possible to find a value of $\overline{R}_{2\times}$ that eliminates the time variation of λ_{eff} within GCMs since the slope of the $\overline{H}$–$\overline{T}$ regression varies over decades to centuries following an abrupt CO_2 change (e.g., Fig. 7; see Andrews et al. 2012b). However, in the regional feedbacks formulation, the time variation of λ_{eff} can be understood simply in terms of a constant $\overline{R}_{2\times}$ (for fixed CO_2), constant $\lambda(r)$ and an evolving surface warming pattern over decadal and longer time scales.

Equation (12) suggests that the slope of the $\overline{H}$–$\overline{T}$ regression is not a measure of λ_{eq} but is, instead, a measure of the strength of feedbacks in those regions where surface temperatures are changing most rapidly at the time when the regression is performed. For example, regression performed over the linear equilibration period—characterized by warming over high-latitude oceans where feedbacks are less negative than average (Figs. 3c,d and 5a)—produces an estimate of λ_{eq} that is less negative than it should be and a corresponding estimate of $\overline{R}_{2\times}$ that is too low (solid line in Fig. 7). Thus, regression methods can be expected to provide biased estimates of λ_{eq} and $\overline{R}_{2\times}$, where the degree of bias is dependent on both the geographic structure of $\lambda(r)$, which varies widely across models (e.g., Zelinka and Hartmann 2012), and on the time scale over which the regression is performed.

We emphasize that extrapolation of the $\overline{H}$–$\overline{T}$ regression to the $\overline{T}$ axis may still yield an accurate estimate of $\overline{T}_{2\times}$ if the regression is performed over the linear equilibration period (Fig. 7). However, regression-based estimates of $\overline{T}_{2\times}$ performed over the period in which $\overline{H}$ evolves nonlinearly with $\overline{T}$ will be inherently biased. For example, within CCSM4, regression over the first 150 years following the abrupt CO_2 doubling (not shown) underestimates $\overline{T}_{2\times}$ by about 0.3°C, compared to regression over the linear equilibration period (solid regression line over years 109–309 in Fig. 7). An implication is that, since the abrupt CO_2-quadrupling integrations included in the Coupled Model Intercomparison Project phase 5 (CMIP5) (Taylor et al. 2012) archive are only 150 years in length, their corresponding regression-based estimates of $\overline{T}_{2\times}$

(e.g., Andrews et al. 2012b) may be systematically biased low.

We note that since our value of $\overline{R}_{2\times}$ is an estimate of the traditional, stratosphere-adjusted CO_2 forcing (see appendix A), it is possible that we have misdiagnosed λ_{eff} to some extent. However, our value of $\overline{R}_{2\times}$ is similar to reported estimates of the troposphere-adjusted forcing within CCSM3 (see Webb et al. 2013, and references therein), perhaps suggesting a relatively small role for nonfeedback cloud adjustments and little difference between these two forcing measures within this model. Overall, our findings highlight the importance of fixed surface temperature experiments (e.g., Shine et al. 2003; Hansen et al. 2005) for calculation of the troposphere-adjusted CO_2 forcing since they avoid the biases associated with regression methods.

Recently, Winton et al. (2010) have proposed an alternative interpretation of $\overline{T}_{\text{eff}}$ in terms of a time-dependent "efficacy of ocean heat uptake" that arises due to its geographic structure, analogous to the distinct efficacies of different radiative forcing agents (Hansen et al. 1997, 2005; Yoshimori and Broccoli 2008). In this view, global ocean heat uptake $\overline{H}$ can be thought of as an effective forcing on the surface components of the climate system, equal to $\varepsilon\overline{H}$ (where ε allows for nonunitary efficacy), such that global surface temperature evolves according to a mixture of radiative forcing and heat exchange with the deep ocean. The relationship between our approach and that of Winton et al. (2010) can be seen by amending the global energy balance:

$$\varepsilon(t)\overline{H}(t) = \lambda_{\text{eq}}\overline{T}(t) + \overline{R}(t). \tag{14}$$

From this perspective, the global climate feedback is assumed to have a constant value λ_{eq}, and the time-varying relationship between $\overline{H}$ and $\overline{T}$ is driven solely by nonunitary $\varepsilon(t)$. The $\overline{H}$–$\overline{T}$ regression in Fig. 7 then has a slope equal to $\lambda_{\text{eq}}/\varepsilon$.

From our perspective, the time-varying relationship between $\overline{H}$ and $\overline{T}$ is driven, instead, by the convolution of regional feedbacks and evolving spatial patterns of surface warming. Since this behavior is subsumed within ε, ε itself may be understood through the regional feedbacks formulation. Combining Eqs. (5) and (14) gives an expression for efficacy in terms of regional properties:

$$\varepsilon(t) = \underbrace{\frac{\overline{H(r,t)/\lambda(r)}}{\overline{H}(t)/\lambda_{\text{eq}}}}_{\text{(i)}} + \underbrace{\frac{\overline{\$\,\square F(r,t)/\lambda(r)}}{\overline{H}(t)/\lambda_{\text{eq}}}}_{\text{(ii)}} - \underbrace{\frac{\overline{R(r,t)/\lambda(r)} - \overline{R}(t)/\lambda_{\text{eq}}}{\overline{H}(t)/\lambda_{\text{eq}}}}_{\text{(iii)}}. \tag{15}$$

Term (i) can be interpreted as the contribution to ε arising from a geographic pattern of ocean heat uptake acting on a geographic pattern of regional feedbacks—ocean heat uptake occurring preferentially in regions of less-negative local feedbacks, such as the Southern Ocean, drives ε toward values greater than one. Note that in the limit of spatially uniform $\lambda(r)$ (equal to λ_{eq} in all regions), term (i) approaches unity.

Term (ii) in Eq. (15) can be interpreted as the contribution to ε arising from changes in the dynamical transport of energy between regions of different local feedback strengths and can thus be described as an "efficacy of heat transport."[2] The transport of energy preferentially out of regions of more-negative feedbacks into regions of less-negative feedbacks drives ε toward a higher value. In the limit of spatially uniform $\lambda(r)$, term (ii) approaches zero. Together, terms (i) and (ii) show that slow variations in the geographic patterns of ocean heat uptake and transport may drive changes in ε over decades to centuries (Fig. 7), consistent with Winton et al. (2010) and Bitz et al. (2012).

Finally, term (iii) in Eq. (15) can be interpreted as the contribution to ε arising from a geographic pattern of radiative forcing acting on a geographic pattern of regional feedbacks and, thus, represents the traditional concept of "efficacy of climate forcing" (Hansen et al. 1997, 2005; Yoshimori and Broccoli 2008). Here ε is driven toward a higher value when stronger forcing occurs preferentially in regions of less-negative feedbacks, consistent with the arguments of Boer and Yu (2003b). In the limit of spatially uniform $\lambda(r)$, term (iii) approaches zero.

Therefore, ε is fundamentally dependent on $\lambda(r)$. Moreover, ε can be interpreted as a pure "ocean heat uptake efficacy" only when terms (ii) and (iii) are negligible; in general, dynamical heat transport changes and a spatial pattern of radiative forcing are also contributors to ε through their preferential actuation of feedbacks within particular regions. However, a near constant ε is an effective characterization of the

[2] We note that the ocean heat transport component of term (ii) may be naturally combined with the ocean heat uptake efficacy, as in Winton et al. (2010).

behavior of λ_{eff} over the period of slow adjustment toward equilibrium with a fixed radiative forcing (solid line in Fig. 7). This period is characterized by a slow decrease in high-latitude ocean heat uptake (Winton et al. 2010; Bitz et al. 2012), resulting in the emergence of a spatially fixed pattern of polar amplified warming (Fig. 3c) and thus a constant $\overline{H}$–$\overline{T}$ slope through Eq. (12).

5. Summary and conclusions

All observation-based estimates and many model-based estimates of climate sensitivity rely on using the global-mean energy budget and global-mean temperature to calculate an effective climate sensitivity $\overline{T}_{\text{eff}}$. Our central finding is that the time variation of $\overline{T}_{\text{eff}}$ appears to be fundamentally controlled by the geographic pattern of (approximately time invariant) regional climate feedbacks and the time-evolving pattern of surface warming. In turn, the spatial structure of surface warming depends on a variety of factors [Eq. (5)]—the patterns of radiative forcing, ocean heat uptake, heat transport, and the regional feedbacks themselves; the regional feedbacks depend on the local physics linking the surface temperature change and TOA radiative response. Radiative forcing, ocean heat uptake, and heat transport drive values of $\overline{T}_{\text{eff}}$ that depend on their spatial structures (through the actuation of regional feedbacks). This leads to the apparent efficacy of ocean heat uptake (Winton et al. 2010) and may contribute to the apparent efficacies of different radiative forcing agents reported in previous studies (e.g., Hansen et al. 1997; Boer and Yu 2003b; Hansen et al. 2005; Yoshimori and Broccoli 2008).

The most important assumptions are that regional feedbacks can be approximated as local, linear, and constant in time. While we do not expect these assumptions to hold in all regions or over large surface temperature changes, they appear to be sufficient for the calculation of $\overline{T}_{\text{eff}}$ within a fully coupled general circulation model (CCSM4) forced by an abrupt CO_2 doubling. However, the time evolution of $\overline{T}_{\text{eff}}$ is not fully accounted for by Eq. (8), particularly over the first few decades of the integration. This can be primarily attributed to the global effective SW feedback (Fig. 2a), suggesting that a source of time variation in either the SW cloud or surface albedo feedbacks has been neglected—plausibly because of a breakdown of our local, linear, time-invariant feedback assumptions, or because of errors in the kernel-calculated feedback pattern.

The effective climate sensitivity $\overline{T}_{\text{eff}}$ is found to be lower than the equilibrium climate sensitivity $\overline{T}_{2\times}$ under transient warming: on decadal time scales, warming of the low-latitude oceans actuates strongly negative (stabilizing) regional feedbacks, leading to a low value of $\overline{T}_{\text{eff}}$; on centennial and longer time scales, a pattern of polar amplified warming emerges, actuating less-negative and even positive (destabilizing) high-latitude feedbacks, driving $\overline{T}_{\text{eff}}$ toward higher values until global climate equilibrium is attained. These basic patterns of change are seen in many GCMs, suggesting that the general results are robust.

The basic principles are also highly robust: regionally varying feedbacks are an inevitable result of the earth's distinct climatic zones, and an evolving pattern of warming is inevitable given the different response times of land, ocean, and sea ice. Of particular relevance for the near-future climate evolution are the geographic variations in ocean dynamics, and resulting ocean heat uptake and transport, that regulate regional changes on time scales ranging from decades to centuries. These principles were demonstrated in a minimalist model, which was also used to highlight the behavior of the global-mean energy–temperature relationship at different stages of the evolving climate response.

In contrast to our local definition, most studies define climate feedbacks with respect to the global-mean surface temperature. An implication of our result is that such feedbacks must in general be interpreted as "effective" quantities that reflect the particular pattern of surface warming over which they are estimated. This result has several important consequences for the estimation and interpretation of climate feedbacks and climate sensitivity. Within models, estimates of climate feedbacks based on transient warming scenarios (e.g., Soden and Held 2006; Zelinka and Hartmann 2012) can be expected to produce different spatial effective feedback patterns, and a different global effective feedback, than those estimates based on equilibrium scenarios (e.g., Shell et al. 2008; Bitz et al. 2012; also see Fig. 4c). Defining local feedbacks with respect to local surface temperature change avoids this time dependence and is arguably a more natural and consistent measure of the local radiative response to warming.

In observational studies, the time variation of $\overline{T}_{\text{eff}}$ impedes our ability to place constraints on the long-term evolution of global climate. Our results, and most others we are aware of (e.g., Winton et al. 2010), show $\overline{T}_{\text{eff}} < \overline{T}_{2\times}$, which raises the possibility that observed estimates of $\overline{T}_{\text{eff}}$ from the modern climate state might also represent an underestimate of the true equilibrium climate sensitivity. However, the degree to which $\overline{T}_{\text{eff}}$ can vary depends critically on the geographic structure of $\lambda(r)$, and it is possible that $\overline{T}_{\text{eff}}$ will show little future evolution if the meridional feedback structure is substantially more flat than that found within CCSM4 (Fig. 5). A substantial challenge for transient global climate prediction is knowing how $\overline{T}_{\text{eff}}$ will evolve over time, which requires

an accurate representation of regional circulations and feedbacks within climate models.

The potential for different types of climate change to be governed by distinct λ_{eff} and $\overline{T}_{\text{eff}}$ greatly complicates the comparison of climate change from different periods. For instance, the climate response to abrupt forcing changes, such as volcanic eruptions, mainly provides a measure of the effective global feedback associated with the rapid adjustments over land and sea ice and, thus, it provides little information about how the global feedback may evolve over long time scales. It might seem appealing, then, to determine the climate response to very slow forcing changes, such as the orbital and greenhouse gas changes between the Last Glacial Maximum and present day, as a near-equilibrium measure of global feedback ($\lambda_{\text{eff}} \approx \lambda_{\text{eq}}$). However, as these periods are driven by distinct patterns of forcing and ocean heat uptake, those equilibrium feedbacks may have operated on a temperature pattern that differed considerably from those associated with present and near-future climate changes (e.g., Crucifix 2006). Bayesian approaches that combine multiple observations of climate change from different periods to derive narrower bounds on climate sensitivity (e.g., Annan and Hargreaves 2006) are predicated on the assumption that each estimate is providing information about the same global climate feedback: thus they are called into question by the finding that λ_{eff} depends fundamentally on the spatial warming pattern in each period.

The regression of global TOA energy flux on global surface temperature is a widely used method to simultaneously estimate the equilibrium global climate sensitivity, feedbacks, and radiative forcing in models and observations. We argue that the regression slope should be interpreted as a measure of the local feedbacks weighted by the rate of local surface temperature change [Eq. (12)] and, thus, that global regression methods can be expected to provide an estimate of the global climate feedback that is biased toward those regions that are changing most rapidly at the time the regression is performed.[3] Correspondingly, the $\overline{H}$-axis intercept calculated by regression methods likely represents a misdiagnosis of the radiative forcing (Figs. 6d and 7). Moreover, linear regression over the period in which $\overline{H}$ evolves nonlinearly with $\overline{T}$ (approximately the first century following an abrupt CO_2 change) likely results in an underestimate of the equilibrium climate sensitivity.

[3] Regression of local TOA flux on local temperature (e.g., Crook et al. 2011) may still provide an accurate estimate of the local feedback and forcing, provided that the regression is performed over a small enough region such that $\lambda(r)$ is approximately uniform.

Finally, our focus has been on an idealized instantaneous CO_2-doubling scenario, which cleanly separates the various time scales of climate response and facilitates identification of the mechanisms of λ_{eff} variation within CCSM4. In more realistic forcing scenarios, where climate forcing is ramped more slowly and a range of radiative forcing agents are included, a different λ_{eff} is expected. The good agreement between λ_{eff} calculated by regional feedbacks and diagnosed by global energy balance suggests that the regional climate feedbacks framework is a powerful tool for calculating and understanding the time variation of λ_{eff} under a range of forcing scenarios and models. Moreover, a redefinition of climate feedbacks in terms of local temperature change eliminates the influence of the spatial pattern of warming and may thus permit greater insight into the causes of the spread in future climate projections across climate models.

Acknowledgments. This research received support from a James S. McDonnell Foundation Postdoctoral Fellowship to KCA and National Science Foundation Grants OCE-0256011 (KCA and CMB) and ARC-0909313 (CMB). We gratefully acknowledge Gokhan Danabasoglu for the CCSM4 integration and Karen Shell for providing the radiative kernels. We thank Marcia Baker, Aaron Donohoe, Ian Eisenman, Nicole Feldl, Dargan Frierson, Yen-Ting Hwang, John Marshall, Raymond Pierrehumbert, Gavin Schmidt, Karen Shell, LuAnne Thompson, and Michael Winton for illuminating discussions, two anonymous reviewers for their valuable suggestions, and Brian Soden, the editor.

APPENDIX A

Calculation of CO_2 Radiative Forcing

We calculate the global radiative forcing from CO_2 doubling $\overline{R}_{2\times}$ from λ_{eq} calculated with radiative kernels and $\overline{T}_{2\times}$ simulated by the slab ocean model (Bitz et al. 2012). Applying Eq. (1), we estimated $\overline{R}_{2\times} = -\lambda_{\text{eq}}\overline{T}_{2\times} = 3.03\ \text{W m}^{-2}$. Calculating the SW and LW components of the forcing separately gives $\overline{R}^{\text{SW}}_{2\times} = -0.02$ and $\overline{R}^{\text{LW}}_{2\times} = 3.05\ \text{W m}^{-2}$. These forcing values are subject to errors in the kernel-calculated global feedback, which have been estimated to be less than 10% for CO_2 doubling (Shell et al. 2008; Jonko et al. 2012).

Cloud feedbacks have been calculated using the "adjusted cloud radiative forcing" method (Soden et al. 2008; Shell et al. 2008) without accounting for forcing-induced cloud changes that occur independent of the surface temperature response. Thus, $\overline{R}_{2\times}$ should be interpreted here as an estimate of the traditional, stratosphere-adjusted CO_2 radiative forcing.

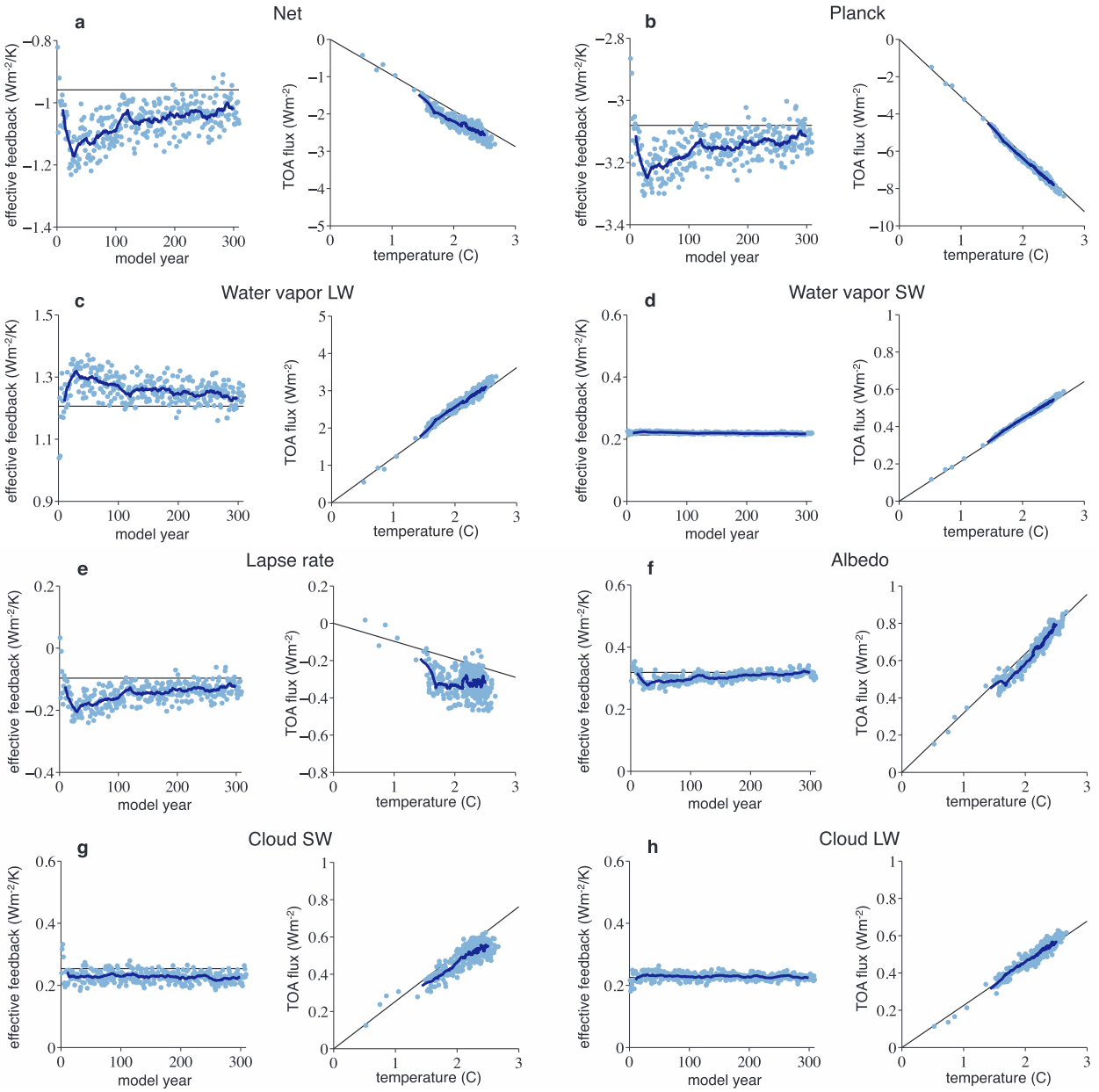

FIG. B1. Global effective climate feedbacks calculated with regional feedbacks [Eq. (8)], and associated global TOA energy flux as a function of global annual-mean surface temperature change, for (a) net (λ_{eff}; sum of all individual effective feedbacks), (b) Planck, (c) LW water vapor, (d) SW water vapor, (e) lapse rate, (f) surface albedo, (g) SW cloud, and (h) LW cloud feedbacks. Light blue dots show individual years, and dark blue lines show the 20-yr running mean. Black lines show the expected evolution if each feedback were constant (equal to its SOM-estimated value) over the simulation.

APPENDIX B

Time Variation of Global Effective Climate Feedbacks

The time evolution of the individual global effective feedbacks and associated global TOA radiation flux is shown in Fig. B1. Global effective feedbacks are calculated by applying Eq. (8) to each of the individual components of the net local feedback $\lambda(r)$ (Fig. 5); the global TAO radiation flux is calculated by multiplying each effective feedback by the global mean surface temperature change in each year. If each effective feedback were constant in time, each TOA radiation flux

would evolve linearly with global-mean surface temperature (black lines in Fig. B1). The net effective feedback, the sum of SW feedbacks, and the sum of LW feedbacks are shown in Fig. 2a.

REFERENCES

Allen, M. R., N. Andranova, B. B. Booth, S. Dessai, D. Frame, and Coauthors, 2007: Observational constraints on climate sensitivity. *Avoiding Dangerous Climate Change,* H. J. Schellnhuber et al., Eds., Cambridge University Press, 281–289.

Andrews, T., and P. M. Forster, 2008: CO_2 forcing induces semi-direct effects with consequences for climate feedback interpretations. *Geophys. Res. Lett.,* **35,** L04802, doi:10.1029/2007GL032273.

——, J. M. Gregory, P. M. Forster, and M. J. Webb, 2012a: Cloud adjustment and its role in CO_2 radiative forcing and climate sensitivity: A review. *Surv. Geophys.,* **33,** 619–635, doi:10.1007/s10712-011-9152-0.

——, ——, M. J. Webb, and K. E. Taylor, 2012b: Forcing, feedbacks and climate sensitivity in CMIP5 coupled atmosphere–ocean climate models. *Geophys. Res. Lett.,* **39,** L09712, doi:10.1029/2012GL051607.

Annan, J. D., and J. C. Hargreaves, 2006: Using multiple observationally-based constraints to estimate climate sensitivity. *Geophys. Res. Lett.,* **33,** L06704, doi:10.1029/2005GL025259.

Baker, M. B., and G. H. Roe, 2009: The shape of things to come: Why is climate change so predictable? *J. Climate,* **22,** 4574–4589.

Bates, J. R., 2007: Some considerations of the concept of climate feedback. *Quart. J. Roy. Meteor. Soc.,* **133,** 545–560.

——, 2010: Climate stability and sensitivity in some simple conceptual models. *Climate Dyn.,* **38,** 455–473.

Bitz, C. M., P. R. Gent, R. A. Woodgate, M. M. Holland, and R. Lindsay, 2006: The influence of sea ice on ocean heat uptake in response to increasing CO_2. *J. Climate,* **19,** 2437–2450.

——, and Coauthors, 2012: Climate sensitivity in the Community Climate System Model, version 4. *J. Climate,* **25,** 3053–3070.

Boer, G. J., 2011: The ratio of land to ocean temperature change under global warming. *Climate Dyn.,* **37,** 2253–2270.

——, and B. Yu, 2003a: Climate sensitivity and climate state. *Climate Dyn.,* **21,** 167–176.

——, and ——, 2003b: Climate sensitivity and response. *Climate Dyn.,* **20,** 415–429.

Colman, R. A., and B. J. McAvaney, 2008: On tropospheric adjustment to forcing and climate feedbacks. *Climate Dyn.,* **36,** 1649–1658.

Crook, J. A., P. M. Forster, and N. Stuber, 2011: Spatial patterns of modeled climate feedback and contributions to temperature response and polar amplification. *J. Climate,* **24,** 3575–3592.

Crucifix, M., 2006: Does the last glacial maximum constrain climate sensitivity? *Geophys. Res. Lett.,* **33,** L18701, doi:10.1029/2012GL053872.

Danabasoglu, G., and P. R. Gent, 2008: Equilibrium climate sensitivity: Is it accurate to use a slab ocean model? *J. Climate,* **22,** 2494–2499.

Edwards, T. L., M. Crucifix, and S. P. Harrison, 2007: Using the past to constrain the future: How the palaeorecord can improve estimates of global warming. *Prog. Phys. Geogr.,* **31,** 481–500.

Forster, P. M. D., and J. M. Gregory, 2006: Diagnosing the climate sensitivity and its components from earth radiation budget data. *J. Climate,* **19,** 39–52.

——, and K. E. Taylor, 2006: Climate forcings and climate sensitivities diagnosed from coupled climate model integrations. *J. Climate,* **19,** 6181–6194.

Gent, P. R., and Coauthors, 2011: The Community Climate System Model, version 4. *J. Climate,* **24,** 4973–4991.

Gregory, J. M., 2000: Vertical heat transports in the ocean and their effect on time-dependent climate change. *Climate Dyn.,* **16,** 501–515.

——, and M. J. Webb, 2008: Tropospheric adjustment induces a cloud component in CO_2 forcing. *J. Climate,* **21,** 58–71.

——, and Coauthors, 2004: A new method for diagnosing radiative forcing and climate sensitivity. *Geophys. Res. Lett.,* **31,** L03205, doi:10.1029/2003GL018747.

Hansen, J., M. Sato, and R. Ruedy, 1997: Radiative forcing and climate response. *J. Geophys. Res.,* **102,** 6831–6864.

——, and Coauthors, 2005: Efficacy of climate forcings. *J. Geophys. Res.,* **110,** D18104, doi:10.1029/2005JD005776.

Hegerl, G. C., and Coauthors, 2007: Understanding and attributing climate change. *Climate Change 2007: The Physical Science Basis,* S. Solomon et al., Eds., Cambridge University Press, 663–745.

Held, I. M., M. Winton, K. Takahashi, T. Delworth, F. Zeng, and G. Vallis, 2010: Probing the fast and slow components of global warming by returning abruptly to preindustrial forcing. *J. Climate,* **23,** 2418–2427.

Holland, M. M., and C. M. Bitz, 2003: Polar amplification of climate change in the coupled model intercomparison project. *Climate Dyn.,* **21,** 221–232.

——, ——, and B. Tremblay, 2006: Future abrupt reductions in the summer arctic sea ice. *Geophys. Res. Lett.,* **33,** L23503, doi:10.1029/2006GL028024.

Jonko, A. K., K. M. Shell, B. M. Sanderson, and G. Danabasoglu, 2012: Climate feedbacks in CCSM3 under changing CO_2 forcing. Part I: Adapting the linear radiative kernel technique to feedback calculations for a broad range of forcings. *J. Climate,* **25,** 5260–5272.

Kay, J. E., M. M. Holland, C. M. Bitz, E. Blanchard-Wrigglesworth, A. Gettelman, A. Conley, and D. Bailey, 2012: The influence of local feedbacks and northward heat transport on the equilibrium Arctic climate response to increased greenhouse gas forcing in coupled climate models. *J. Climate,* **25,** 5433–5450.

Kiehl, J. T., C. A. Shields, J. J. Hack, and W. D. Collins, 2006: The climate sensitivity of the Community Climate System Model, version 3 (CCSM3). *J. Climate,* **19,** 2584–2596.

Kirkman, C., and C. M. Bitz, 2011: The effect of the sea ice freshwater flux on southern ocean temperatures in CCSM3: Deep ocean warming and delayed surface warming. *J. Climate,* **24,** 2224–2237.

Knutti, R., and G. C. Hegerl, 2008: The equilibrium sensitivity of the earth's temperature to radiation changes. *Nat. Geosci.,* **1,** 735–743.

——, T. F. Stocker, F. Joos, and G.-K. Plattner, 2002: Constraints on radiative forcing and future climate change from observations and climate model ensembles. *Nature,* **416,** 719–723.

Levitus, S., J. I. Antonov, J. Wang, T. L. Delworth, K. W. Dixon, and A. J. Broccoli, 2001: Anthropogenic warming of earth's climate system. *Science,* **292,** 267–270.

Li, C., J.-S. von Storch, and J. Marotzke, 2013: Deep-ocean heat uptake and equilibrium climate response. *Climate Dyn.,* **40,** 1071–1086, doi:10.1007/s00382-012-1350-z.

Manabe, S., R. J. Stouffer, M. J. Spelman, and K. Bryan, 1991: Transient response of a coupled atmosphere–ocean model to gradual changes of atmospheric CO_2. Part I: Annual mean response. *J. Climate,* **4,** 785–818.

Murphy, D. M., S. Solomon, R. W. Portmann, K. H. Rosenlof, and P. M. Forster, and T. Wong, 2009: An observationally based energy balance for the earth since 1950. *J. Geophys. Res.,* **114,** D17107, doi:10.1029/2009JD012105.

Murphy, J. M., 1995: Transient response of the Hadley Centre coupled ocean–atmosphere model to increasing carbon dioxide. Part I: Control climate and flux adjustment. *J. Climate,* **8,** 36–56.

Raper, S. C. B., J. M. Gregory, and R. J. Stouffer, 2002: The role of climate sensitivity and ocean heat uptake on AOGCM transient temperature response. *J. Climate,* **15,** 124–130.

Senior, C. A., and J. F. B. Mitchell, 2000: Time-dependence of climate sensitivity. *Geophys. Res. Lett.,* **27,** 2685–2688.

Shell, K. M., J. T. Kiehl, and C. A. Shields, 2008: Using the radiative kernel technique to calculate climate feedbacks in NCAR's community atmospheric model. *J. Climate,* **21,** 2269–2282.

Shine, K. P., J. Cook, E. J. Highwood, and M. M. Joshi, 2003: An alternative to radiative forcing for estimating the relative importance of climate change mechanisms. *Geophys. Res. Lett.,* **30,** 2047, doi:10.1029/2003GL01814.

Soden, B. J., and I. M. Held, 2006: An assessment of climate feedbacks in coupled ocean–atmosphere models. *J. Climate,* **19,** 3354–3360.

——, ——, R. Colman, I. M. Shell, J. T. Kiehl, and C. A. Shields, 2008: Quantifying climate feedbacks using radiative kernels. *J. Climate,* **21,** 3504–3520.

Stouffer, R. J., 2004: Time scales of climate response. *J. Climate,* **17,** 209–217.

Taylor, K. E., R. J. Stouffer, and G. A. Meehl, 2012: An overview of CMIP5 and the experiment design. *Bull. Amer. Meteor. Soc.,* **90,** 485–498.

Watterson, I. G., 2000: Interpretation of simulated global warming using a simple model. *J. Climate,* **13,** 202–215.

Webb, M. J., F. H. Lambert, and J. M. Gregory, 2013: Origins of differences in climate sensitivity, forcing and feedback in climate models. *Climate Dyn.,* **40,** 677–707, doi:10.1007/s00382-012-1336-x.

Wigley, T. M. L., and S. C. B. Raper, 2001: Interpretation of high projections for global-mean warming. *Science,* **293,** 451–454.

Williams, K. D., W. J. Ingram, and J. M. Gregory, 2008: Time variation of effective climate sensitivity in GCMs. *J. Climate,* **21,** 5076–5090.

Winton, M., 2006: Amplified arctic climate change: What does surface albedo feedback have to do with it? *Geophys. Res. Lett.,* **33,** L03701, doi:10.1029/2005GL025244.

——, K. Takahashi, and I. M. Held, 2010: Importance of ocean heat uptake efficacy to transient climate change. *J. Climate,* **23,** 2333–2344.

Yoshimori, M., and A. J. Broccoli, 2008: Equilibrium response of an atmosphere–mixed layer ocean model to different radiative forcing agents: Global and zonal mean response. *J. Climate,* **21,** 4399–4423.

Zelinka, M. D., and D. L. Hartmann, 2012: Climate feedbacks and their implications for poleward energy flux changes in a warming climate. *J. Climate,* **25,** 608–624.